Direct Measurements of Energetic Neutral Hydrogen in the Interplanetary Medium

A. Galli and P. Wurz

University of Bern, Physikalisches Institut, CH-3012 Bern, Switzerland

galli@phim.unibe.ch

S. Barabash, A. Grigoriev, R. Lundin, Y. Futaana, H. Gunell, M. Holmström

Swedish Institute of Space Physics, Box 812, SE-981 28 Kiruna, Sweden

E. C. Roelof

Applied Physics Laboratory, John Hopkins University, Laurel, MD 20723-6099, USA

C. C. Curtis, K. C. Hsieh

University of Arizona, Tucson, AZ 85721, USA

A. Fedorov

Centre d'Etude Spatiale des Rayonnements, BP-4346, F-31028 Toulouse, France

D. Winningham, R. A. Frahm

Southwest Research Institute, San Antonio, TX 7228-0510, USA

R. Cerulli-Irelli

Instituto di Fisica dello Spazio Interplanetario, I-00133 Rome, Italy

P. Bochsler

University of Bern, Physikalisches Institut, CH-3012 Bern, Switzerland

N. Krupp, J. Woch, M. Fraenz

Max-Planck Institut für Aeronomie, D-37191 Katlenburg-Lindau, Germany

To be submitted to ApJ., 2005/2006.

ABSTRACT

We present an analysis of hydrogen energetic neutral atoms (ENAs) measured by the ASPERA-3 instrument on board of Mars Express. We focus on ENAs that have no Martian origin. The energy spectra of these ENAs are all very similar and can be fitted well by a two-component power law. The fluxes, integrated from 0.2 keV to 10 keV, vary between $5 \cdot 10^3$ and 10^5 cm^{-2} sr^{-1} s^{-1}. We checked for possible sources for these ENAs, but we can rule out a planetary origin, a solar wind origin, contamination by UV from UV bright stars, and a contamination by high energy protons. With our present knowledge we conclude that the heliospheric termination shock is the most plausible source region.

Subject headings: interplanetary medium — solar wind — acceleration of particles — plasmas — methods: data analysis — instrumentation: detectors

1. INTRODUCTION

The imaging of energetic neutral atoms (ENAs) has become an established means of remote sensing plasma distributions in planetary and space science (Wurz 2000). Recent examples include the study of Titan's exosphere (Mitchell et al. 2005), the terrestrial ionosphere and interplanetary medium by LENA (Moore et al. 2003), or the heliospheric ENAs by SOHO (Hilchenbach et al. 1998). An energetic neutral atom starts as an ion, which is accelerated by an electromagnetic field until it exchanges its charge with a neutral atom of the ambient gas. It retains its original energy but is not influenced by electromagnetic fields anymore. It leaves the place of its birth on a ballistic trajectory and may reach regions far away from the original population of ions. Among many other applications, ENA imaging has been proposed (Gruntman et al. 2001; Fahr & Scherer 2004) and is planned to be used (McComas et al. 2004) to investigate the boundary of the heliosphere and the interstellar medium itself.

Heliospheric ENAs are predominantly hydrogen neutrals that have been produced on the far side of the termination shock in the inner heliosheath, where the solar wind has been slowed down to subsonic speed. There, ENAs are continually produced by charge exchange between interstellar neutrals and protons from the solar wind or from other ion populations. These processes ought to result in a detectable flux of inward moving ENAs from the inner heliosheath (Gruntman et al. 2001; Fahr & Scherer 2004). Imaging these ENAs and their energy spectra would reduce our considerable uncertainties about the termination shock, the heliosheath surrounding it, and in general about the interaction of the heliosphere with the local interstellar medium.

In this article we present and discuss energy spectra of ENAs measured by the ASPERA-3 instrument on board of the Mars Express spacecraft (Barabash et al. 2004). The neutral

particle detectors of the ASPERA-3 instrument were originally conceived to image ENA fluxes from Mars. But a preliminary evaluation showed in some cases a signal of energetic neutral hydrogen although the NPD sensors were pointed away from Mars, which prompted further research on these particular events. It meant, quite uncommon for a Mars research experiment, that we sampled all data where Mars is well out of the NPD field-of-view. We will present all those ENA measurements with a non-planetary origin and discuss possible explanations. As we will see, a heliospheric origin of these ENA streams cannot be proved for sure, but it is the most plausible explanation.

2.   INSTRUMENTATION

The ASPERA-3 instrument (Barabash et al. 2004) has been designed to study the interaction of the solar wind with the Martian atmosphere and to characterize the plasma and neutral gas environment in the vicinity of Mars. First results have been reported by Lundin et al. (2004).

The ASPERA-3 instrument comprises four different sensors. The Ion Mass Analyser and the Electron Spectrometer to measure local ion and electron densities, respectively, and the Neutral Particle Detector (NPD) and the Neutral Particle Imager (NPI) to detect energetic neutral atoms. The results presented here are restricted to neutral particle measurements. Particular attention has been paid to those NPD data sets where the field-of-view of the sensors is directed away from Mars.

The Neutral Particle Detector consists of two identical sensors NPD1 and NPD2 that are sensitive to ENAs in the energy range of 0.1 to 10 keV using the time-of-flight technique. Each sensor has one start and three stop surfaces that provide an angular resolution of roughly 30° in azimuthal direction and 4° in elevation direction, which is shown in Figure 1.

The energy and the mass of an incident particle can be reconstructed from the time of flight between start and stop surface and from the pulse height of the stop signal. Principally, this design enables us to distinguish oxygen from hydrogen in the Martian exosphere.

EDITOR: PLACE FIGURE 1 HERE.

3. DATABASE

The database for the search for ENA fluxes without planetary origin comprises all data sampled in RAW and in TOF operation mode of NPD (Barabash et al. 2004) where a Martian origin can be excluded, i.e., Mars is outside the field-of-view of NPD. There are several time periods from July 2003 until March 2005, which are useful for this research topic. There also exists a so called BINNING mode, but the TOF information is compressed into only 16 instead of 256 bins in this mode. The time of flight information thus is not sufficient to obtain a reliable energy spectrum and therefore BINNING mode data have been omitted from this analysis.

This database includes all data sets from the cruise phase and the few data sets from Mars orbit where the angle between the Mars limb and the closest edge of the field-of-view is larger than 45°. All including, there are 10 different dates from the cruise phase and 102 dates from the Mars orbit that have been found to meet our criterion.

Figure 2 gives an overview of four arbitrarily chosen measurement locations in the ecliptic reference frame during cruise and orbit phase. The black ellipses are the Earth and Mars orbits, the wedge-shaped sectors indicate the fields-of-view of the two NPD sensors for the indicated dates of observation.

EDITOR: PLACE FIGURE 2 HERE.

4. SPECTRUM RECONSTRUCTION

The NPD sensor accumulates time-of-flight information of incoming ENAs in steps of one second, but 10 minutes of integration time are generally required to obtain a TOF spectrum with reasonably small random fluctuations. This implies that we have discarded any short-scale time variations in our analysis. Figure 3 gives an example of a raw TOF spectrum (top panel), which has been converted into an energy spectrum (bottom panel). The value of each TOF bin corresponds to the average count rate per second.

EDITOR: PLACE FIGURE 3 HERE.

To convert the uncalibrated TOF spectrum into an energy spectrum in units of cm^{-2} sr^{-1} s^{-1} keV^{-1} we assume that all detected ENAs are hydrogen atoms between 0.1 and 10 keV and that all of the six different MCP detectors behave identical. Whereas the latter assumption is justified by laboratory calibration, the first assumption is only justified as long as we are dealing with non-planetary ENAs. The Martian exosphere by contrast is bound to produce oxygen ENAs in abundance as well. The TOF signature of helium ENAs would hardly be discernible from hydrogen, but in interplanetary space the flux intensity of helium ENAs of about 1 keV will be orders of magnitude lower. A possible contribution by helium ENAs to the signals is therefore disregarded in the present analysis.

First, we subtract the noise background (see Appendix for more information) caused by UV photons. If an ENA signal beyond the background is recognizable we apply a low-pass filter (Marshall & Verdun 1990) to eliminate any short period (shorter than 10 TOF bins) signal, including the harmonic noise caused by the sensor electronics (see e.g. Figure 3). We then invert the instrument response by searching for an optimal fit function, which, applied to

the instrument response function, comes closest to the observed TOF spectrum using a least-squares method. Finally, to convert the count rates of the reconstructed time-of-flight spectrum into differential fluxes, the count rates have to be divided by the product of the energy-dependent detection efficiency, geometrical factor, and the corresponding energy range of the TOF bin.

We retrieve from the reconstruction only four parameters that have been fitted to the energy spectrum between 0.2 and 10 keV: the slope at low energies (a_1), the slope at high energies (b_1), the place of the roll-over (c), and the integral flux. In the subsequent discussion, the integral flux will be understood to cover the energy range from 0.2 keV to 10 keV unless specified otherwise. Although particles with energies between 0.1 and 0.2 keV are detected, we have chosen 0.2 keV as lower cut-off, because the efficiency for energies between 0.1 and 0.2 keV is not well known. Integrating over this energy range would result in highly uncertain flux estimates (see Appendix for further information). We find, within the range of uncertainty, that the vast majority of the resulting energy spectra can adequately be parameterized by a simple two-composite power law in the range between 0.2 and 10 keV, according to

$$f(E) = \begin{cases} a_0 E^{a_1} & \text{if } E < c, \\ b_0 E^{b_1} & \text{if } E \geq c. \end{cases} \tag{1}$$

5. OBSERVATIONS

The majority of TOF spectra in our database (a total of 205 spectra) of non-planetary ENA streams show only noise or they have an insufficient signal-to-noise ratio so that one cannot put any constraints on the reconstructed energy spectra. Our detection limit for ENA signals lies at $\sim 5 \cdot 10^3$ cm^{-2} sr^{-1} s^{-1}. In the subsequent discussion we shall first give an overview of all 205 measurements before concentrating on the occasions where an ENA

signal is clearly visible.

Figure 4 shows the integral fluxes as a function of observation date for all measurements from the database, including ill-defined spectra and measurements with no signal at all. Obviously, there are long observation gaps. During cruise phase the sensor was switched on only on a few occasions. After Mars orbit insertion the sensor was directed to Mars for most measurements, since the primary goal of ASPERA-3 was to study the Martian atmosphere. The fluxes seem to decrease with time and the vast majority of measurements from 2005 shows no signal at all with the exception of the subset mentioned in Section 5.2. Figure 4 shows that flux variations from the detection limit up to 10^5 cm^{-2} sr^{-1} s^{-1} can occur on time scales of months. It is difficult to tell temporal from spatial variations with our sparse data set. Generally, the pointing direction of the field-of-view also changes from one observation opportunity to the next. Beside the long observation gaps, the spatial distribution of the observations is not favorable either. Virtually all useful data were measured when the field-of-view of NPD was close to the ecliptic plane. After all, ASPERA-3 was designed as a Mars exploration experiment. It was not set up to search for non-planetary ENA signals.

<p style="text-align:center">EDITOR: PLACE FIGURE 4 HERE.</p>

In short, the integral fluxes show big variations, but these are either stochastic or on time scales shorter than we can resolve with the few useful datasets.

5.1. The Typical ENA Spectrum

Figure 5 shows a typical example of an energy spectrum, reconstructed from NPD2 data measured on 2003 July 10 during the cruise phase. The signal is not of planetary origin

since all planets are too far away and outside the field-of-view. It is a typical example insofar that from the 66 measurements having a sufficiently high signal-to-noise ratio 51 result in energy spectra that are appropriately characterized by a two-composite power law with a moderate decrease at low energies, a roll-over somewhere close to 0.8 keV, and a steeper decrease at higher energies.

EDITOR: PLACE FIGURE 5 HERE.

If one displays the parameter for the roll-over of all available 66 spectra on one single plot one recognizes that a few data points lie far away from the typical value found in the early measurements during cruise phase. Figure 6 shows the position of the roll-over, which is the best-defined parameter in the analysis. It can reasonably be defined even for the few cases where the energy spectrum does not follow a two-composite power law but shows one single peak.

EDITOR: PLACE FIGURE 6 HERE.

5.2. Outliers Or Martian Contamination?

Looking at Figure 6 we find that the data obtained during cruise phase show a consistent result. Afterwards the variation of the spectral parameters increases significantly. This may indicate an instrumental degradation, but it is more likely that Mars acts as a source of contamination once Mars Express is in orbit, although all data sets where Mars gets near to the field-of-view have been excluded from our analysis.

From the 66 data sets displayed in Figure 6 we selected 51 spectra, which are displayed in Figure 7. All of them belong to the time span between July 2003 and May 2004. Among

the numerous measurements from January to March 2005 only 8 show a recognizable ENA signal. However, the corresponding energy distribution of these fluxes does not fit to the typical spectrum (see Figure 5 for reference). It shows a peak between 1 and 1.3 keV which is similar to spectra obtained from Mars limb observation (see Figure 8). Therefore, these measurements are excluded from further discussion. Another reason to disregard these 8 events is the fact that all of them are measured with the field-of-view co-aligned to the Parker angle of the interplanetary magnetic field. A solar wind induced signal is therefore plausible for this sub dataset, contrary to the majority of non-planetary signals discussed in Section 5.3.

5.3.   Statistics of Non-Planetary ENA Signals

In the following discussion we shall exclude the eight events in 2005 from the evaluation, as well as the other few events with a spectral shape that cannot be characterized by a two-composite power law and a poor signal-to-noise ratio. This leaves us with 51 spectra that seem to belong to one single spectrum class. The spectral parameters of the remaining data sets are shown in Figure 7, together with the median values. The spectrum shape is described by

$$f(E) = \begin{cases} a_0 E^{-1.6} & \text{for } E < 0.77 \text{ keV}, \\ b_0 E^{-3.3} & \text{for } E \geq 0.77 \text{ keV}, \end{cases} \qquad (2)$$

whereby the statistical 1σ error bars of the average values for the data in Figure 7 range between $-2.1 < a_1 < -1.1$, 0.55 keV $< c < 1.0$ keV, $-3.9 < b_1 < -2.7$, and a_1, b_1 ,and c are defined in Equation 1.

EDITOR: PLACE FIGURE 7 HERE.

6.   DISCUSSION

Let us shortly discuss possible explanations for the ENA signal presented in the previous section. Some explanations can be ruled out, upon others we may never be able to reach a definitive conclusion with the available database.

6.1.   Comparison to Martian ENA Spectra

There is a general difference between the typical non-planetary spectrum shown in Figure 5 and signals of Martian ENAs. The latter often show energy spectra with a distinct peak or a roll-over at high energies well above 1 keV, whereas the well-defined spectra of non-planetary ENA events share a roll-over between 0.7 to 0.9 keV. We find that the integral fluxes of ENAs produced by interactions with the Mars atmosphere may reach several 10^6 cm^{-2} sr^{-1} s^{-1}, which is an order of magnitude higher than the highest flux measured in the case of non-planetary ENA signals (see Figure 4).

Figure 8 illustrates one of many occasions where the field-of-view has approached the Mars limb and a stream of ENAs is detected that obviously originate from Mars. This is the reason why any signal measured when the field-of-view was closer to the Martian limb than 45° has been excluded from our study in the first place. In the case of Figure 8, the energy spectrum with a distinct peak at 1 keV hints to solar wind protons that have been neutralized in the Martian atmosphere (Futaana et al. 2005). Such a signal can be easily told from non-planetary spectra as listed in Figure 7. It has, however, a certain similarity to the ENA signals in 2005 with an untypical high roll-over (see Section 5.2), which after all might reflect a Martian contamination as well.

EDITOR: PLACE FIGURE 8 HERE.

6.2.   UV Sensitivity

Stars produce high fluxes of UV-photons which might - by interaction with the start and stop surfaces of the NPD detector - give us a mock signal. The Sun is in all measurements outside the field-of-view but we needed to check if single stars or the galaxy as a whole could be the source of the unexplained neutral streams.

This question is answered by the measurement on 2003 July 13. By a stroke of luck α Cen, the closest star to our Sun, wandered across the field-of-view of the NPD1 detector. Figure 9 shows the field-of-view and the position of the brightest stars at two different times during the observation period, below are the registered count rates and the average TOF spectra. As a matter of fact, UV photons cause the noise floor in the TOF spectra and passing nearby stars raise this floor by factors 4...5, but they do not produce a peak in the TOF spectrum that could be mistaken for an ENA signal.

EDITOR: PLACE FIGURE 9 HERE.

In summary, not one of the 51 events mentioned in Section 5.3 can be related to a nearby star. Stellar UV-light does not produce a TOF spectrum that could be mistaken with signals such as shown in Figure 5. The global spatial pattern of the integral fluxes (see Figure 12 in Section 6.4) is not consistent with nearby stars or the galactic center as source regions of the signals.

6.3.   Suprathermal Ions And Parker Angle

There is - besides the anomalous energy spectrum - another reason to separate the eight events (see Section 5.2) in 2005 from the typical ENA measurements. They are aligned with the direction of the magnetic field of the solar wind. Most other signals, those measured

during cruise phase in particular, show no correlation with the direction of the Parker angle at the given heliocentric distance. This is illustrated by Figure 10.

EDITOR: PLACE FIGURE 10 HERE.

For those events where the NPD aperture actually is co-aligned with the interplanetary magnetic field, suprathermal ions of 100 keV seemed to be a possible explanation. Energetic ions created at a distant shock travel along the magnetic field lines and enter the NPD instrument. These ions are too energetic to be eliminated by the electric field for ion suppression in the collimator, which sweeps away all ions below 70 keV. The energetic ions then hit the start surface and produce secondary particles that could be mistaken for energetic neutral atoms hitting the stop surfaces. However, simulations with the SRIM software (Ziegler et al. 1996) lead us to conclude that such so-called suprathermal protons of 100 keV are no reasonable explanation for our signals. It would take a flux of $10^5..10^6$ cm^{-2} sr^{-1} s^{-1} of suprathermal ions to mock an ENA signal of 10^4 cm^{-2} sr^{-1} s^{-1}. Moreover, Figure 11 shows that neither the TOF nor the energy spectrum of the backscattered ions gets close to the typical non-planetary ENA signal (compare to Figure 5, for example).

EDITOR: PLACE FIGURE 11 HERE.

6.4.   A Spatial Pattern

There is one remarkable correlation that cannot be explained by an observational bias. The ENA signals show a geographic pattern, with a preferred direction lying between 30° and 90° ecliptic longitude. The correlation of integral flux with ecliptic longitude is statistically

significant at the 95% confidence level for a Spearman rank correlation test applied to 12 data bins of 30° each (shown in the lower panel of Figure 12). This is true whether we restrict the analysis to the well-defined 51 spectra or if we include all 205 measurements.

Figure 12 shows the variation of integral flux with ecliptic longitude. The Sun is moving compared to the local interstellar medium towards 255° with about 25 km s^{-1}. This results in a stream of low energetic hydrogen and helium neutrals flowing from this direction towards the Sun (Witte et al. 2004; Lallement et al. 2005). The ENA signal measured by ASPERA-3 on the other hand seems to increase in integral flux between 30° and 90°, around the Anti-apex direction, while a zone with scarcely any signal expands from 180° to 300°. It is deplorable that so few measurements fall within the region of 0° to 90° ecliptic longitude where the highest fluxes seem to originate from. Nothing can be said about the latitudinal distribution of the signals, as the NPD detector was aligned to the ecliptic plane in virtually all instances.

EDITOR: PLACE FIGURE 12 HERE.

It may be worth considering that Hilchenbach et al. (1998) have published results of energetic hydrogen measurements performed by HSTOF on the SOHO mission. Their instrument had a different energy range (55...80 keV) compared to ASPERA-3. But, consistently with our findings (Figure 12), they also observed a preferred direction of origin for their ENA signal between 70° and 90° ecliptic longitude. The reported integral fluxes (Czechowski et al. 2005) fall within the same order of magnitude as the ENA measurements presented in this work if one assumes a power law decrease between 6 and 60 keV according to $f(E) \sim E^{-3.5}$. Until now, the process that produces the ENA signals reported by Hilchenbach et al. (1998) is not identified with certainty. The spatial and temporal resolution makes it hard to decide between a local, interplanetary (Kota et al.

2001) or a remote, heliospheric origin of the ENAs (Czechowski et al. 2001, 2005).

7.   CONCLUSION

We have detected signals of energetic neutral hydrogen over a time range of 10 months. For the statistical evaluation we have accounted for all data sets where Mars is well out of the field of view, be there a recognizable signal or not. 51 of the 66 energy spectra with a favorable signal-to-noise ratio fit into one single spectrum class

$$f(E) = \begin{cases} a_0 E^{-1.6} & \text{for } E < 0.77 \text{ keV}, \\ b_0 E^{-3.3} & \text{for } E \geq 0.77 \text{ keV}, \end{cases} \tag{3}$$

independent of observation date or pointing direction. The integral flux between 0.2 and 10 keV varies from $5 \cdot 10^3$ up to 10^5 cm^{-2} sr^{-1} s^{-1} either spatially or on small timescales that we cannot resolve. These signals do not correlate with the position of Earth, Mars, Jupiter or Saturn and their spectra look different from typical ENA signals from Mars.

The source of the ENA signal is not identified with confidence yet. There has to be a mechanism that produces neutral hydrogen fluxes in the order of $10^4 \ldots 10^5$ cm^{-2} sr^{-1} s^{-1} with velocities around 400 km s^{-1}. These velocities are an order of magnitude higher than the relative motion of the Sun through the local interstellar cloud and the direction where we measure the highest fluxes of ENA atoms lies between 90° to 180° away from the direction of the interstellar neutral flow and from the galactic center.

Based on our present analysis our conjecture is that we are observing energetic neutral particles that were produced in the area of the heliospheric termination shock. The typical integral flux of several 10^4 cm^{-2} sr^{-1} s^{-1} is about an order of magnitude higher than fluxes derived from theoretical models (Fahr & Scherer 2004; Gruntman et al. 2001), but is consistent with ENA measurements done by HSTOF on SOHO (Czechowski et al. 2005).

The main objection to the heliospheric explanation is the temporal variation of the integral fluxes for the same region (check the upper panel in Figure 12). Generally, the distance to the source region of the ENA signal could be estimated if we could determine the timescale of flux variations. A heliospheric origin of the observed ENAs requires this timescale to be longer than a few months, since an ENA of energy 0.3 keV takes about 2 years to travel the distance of 100 AU from the termination shock to the inner solar system, whereas a 2 keV ENA takes only 9 months. Therefore, even an ENA event that is a short pulse at the termination shock will be spread out in time during its propagation to the detector over many months. If the signal is found to vary over a timescale of one month or less, the ENA signal has to originate from a localized source within a few AU distance, and processes in the local solar wind, such as CIRs, would be needed to explain our observations. Unfortunately, there are only two occasions where we observe the same direction more than once within one month. The first one are the dozen measurements between $320°$ and $335°$ ecliptic longitude in Figure 12 that have been measured during July 2003 in cruise phase. The spectrum remains the same but the integral flux dropped from $6.6 \cdot 10^4$ cm^{-2} sr^{-1} s^{-1} to $1.0 \cdot 10^4$ cm^{-2} sr^{-1} s^{-1}. But since these were the very first measurements this drop in count rates might also be explained by a water contamination of the active detector surface, which was slowly lost during the first measurements. The only two occasions where a flux below $3 \cdot 10^4$ cm^{-2} sr^{-1} s^{-1} was measured, the integration times were only 15 minutes compared to typically one hour for the other data in July 2003. In any case the time scale of the ENA variations must be longer than days since there was a measurable signal from this direction whenever the detector was operational in July. As far as cruise phase data are concerned, there is no overlapping between regions where a signal was detected and regions where no signal was detected from July to October 2003. The other region that we observe more than once within a month is the one between $30°$ and $40°$ ecliptic longitude. It was covered twice, namely on 2004 January 5 and January 12. The integral flux increased by

a factor of 2.5 within a week. However, in this time span Mars Express approached Mars from 11 to 4 Mars radii and a Martian contamination once more cannot be excluded.

The temporal variability seems easier to be reconciled with a localized solar wind origin, but there are at least two objections against this explanation. First, a solar wind source is inconsistent with the observed direction of origin (see Figure 12). Even if there are energetic protons produced in the vicinity of the NPD detector, for instance due to CIRs, they still need neutral hydrogen atoms to charge exchange in order to be detected as ENAs. Since the interplanetary hydrogen density is higher towards the apex direction of the heliosphere, a localized ENA source would not preferentially be observed from downwind direction. Second, the ENA signal is at least 3 orders of magnitude higher than one would expect if it were caused by protons that have been accelerated in a nearby CIR. The differential flux of ENAs at 1 keV energy that can be locally produced calculates to

$$j_{ENA} = \sigma \cdot \int_{LOS} (n_H \cdot j_P) dl, \tag{4}$$

where j_P is the differential flux intensity of 1 keV protons in units of cm^{-2} sr^{-1} s^{-1} keV^{-1}, $\sigma = 2 \cdot 10^{-15}$ cm^2 is the cross-section for the charge exchange between a 1 keV proton and a thermal hydrogen atom (Gruntman et al. 2001), $n_H = 0.1$ cm^{-3} is the interplanetary hydrogen particle density, and the integral is a line-of-sight integral taken over a typical length scale. For a local source in the inner solar system we set $\int_{LOS} dl = 1$ AU. Equation 4 then yields as a rough estimate for the required proton flux:

$$j_{ENA} = 10^{-3} \cdot j_P \tag{5}$$

Since we typically observe at 1 keV $j_{ENA} = 10^4 cm^{-2}$ sr^{-1} s^{-1} keV^{-1} it would require at least (Eq. 5) a differential flux of $j_P = 10^7 cm^{-2}$ sr^{-1} s^{-1} keV^{-1} 1 keV protons to reproduce our ENA-observations. This gets close to the flux intensity of the solar wind itself, whilst

we are looking away from the Sun! Spectra of high energy protons from CIR events are available, see for instance Desai et al. (1999) for the energy range between 50 keV to 20 MeV. But to our knowledge the energy spectrum of CIR-protons at 1 keV has not been measured yet. If we extrapolate the value at 100 keV found by Desai et al. (1999) down to 1 keV assuming a power law with an exponent of -2 (which seems to be the most extreme case according to Figs. 4 and 6 in Desai et al. (1999)), we find only $j_P = 10^4 cm^{-2}$ sr^{-1} s^{-1} keV^{-1} at 1 keV. This is three orders of magnitude too low.

We have checked that an instrumental effect, such as high energy protons scattering on the start surface, cannot explain the measurements. The Sun always is outside the field-of-view, and the observed ENA signal shows no correlation with the Parker angle of the solar wind. We also have shown that the signal is not caused by UV-photons, the geographical pattern of the signals does not correlate with bright nearby stars or with the galactic center.

It is unclear if ASPERA-3 will sample many more datasets that can be used for the study presented here, since most of the well-defined spectra have been sampled in 2003 during the cruise phase. For the oncoming Venus Express mission it would be favorable to sample more data during the cruise phase and to cover the entire sky. Further insight into ENAs of non-planetary origin will hopefully be provided by NASA's IBEX mission (McComas et al. 2004).

A.   APPENDIX

The estimate of the noise level has a big influence on the resulting energy spectrum. We have verified with numerical simulations of the instrument response that UV photons are the prime source of background in the TOF spectra. The UV photons originate from

resonant backscattering in interplanetary hydrogen (Ly-α emission lines account for 600 Ra) and helium (only 7 Ra), bright nearby stars and the galactic disk increase the UV flux to several 1000 Ra.

The count rates registered in the higher TOF bins from 100 to 256 can be understood as result of a start and a stop signal of two different, uncorrelated photons that have been registered by the sensor almost simultaneously. We also know from calibration that the counter surfaces are insensitive to ENAs below 0.1 keV. Therefore, we use a linear noise model whose parameters are fitted to the count rates in the highest TOF bins from 200 to 256. After subtracting the background, all the bins that correspond to energies below 0.1 keV will be excluded from the analysis, as will be the lowest few TOF bins.

The range of uncertainty is calculated for each bin through the entire reconstruction analysis. The prime sources of error are the counting statistics themselves, the uncertainty in estimating the UV background and the poorly known detection efficiency for atoms at energies below 0.3 keV.

Figure 13 gives an extreme example but also illustrates the solution: Since the error bars for a single energy bin are large it is intuitive to characterize the reconstructed energy spectrum by only a few parameters, which are much better constrained than the values of a single energy bin. The relative uncertainty on the derived parameters amounts to roughly 10% only, which is also shown in Figure 13. Below 0.3 keV the uncertainty of the NPD detection efficiency becomes troublesome, whereas at high energies poor counting statistics is the prime source of uncertainty. The effect of these errors is comparable to the intrinsic energy resolution limit (FWHM criterion applied to the resulting peak for a monoenergetic beam) $\Delta E/E \approx 0.3$ between 0.3 and 1 keV.

Thus, instead of 256 different energy bin values, each of them with considerable uncertainty, we retrieve from the reconstruction only the four parameters mentioned in Section 4.

EDITOR: PLACE FIGURE 13 HERE.

REFERENCES

Barabash, S., et al. 2004, ASPERA-3: Analyser of Space Plasmas and Energetic Ions for Mars Express, 2004mesp.book, 121

Collier, M. R., et al. 2004, Adv.S.R., 34, 166

Czechowski, A., et al. 2001, A&A, 368, 622

Czechowski, A., Hilchenbach M., Hsieh K. C. 2005, A&A, 431, 1061

Desai, M. I., et al. 1999, JGR, 104, 6705

Fahr, H.-J., Scherer, K. 2004, ASTRA 1, 3

Futaana, Y., et al. 2005, Icarus, in press

Grigoriev, A., Barabash, S., Fedorov, A. 2003, ASPERA-3/NPD2 FM2 calibration report, http://aspera-3.irf.se/

Gruntman, M., Roelof, E.C., Mitchell, D.G., Fahr, H.-J., Funsten, H.O., McComas, D.J. 2001, JGR, 106, 15767

Hilchenbach, M., et al. 1998, ApJ, 503, 916

Kota, J., Hsieh, K. C., Jokipii, J. R., Czechowski, A., Hilchenbach, M. 2001, JGR, 106, 24907

Lallement, R., Quémerais, E., Bertaux, J.L., Ferron, S., Koutroumpa, D., Pellinen, R. 2005, Science, 307, 1447

Lundin, R., et al. 2004, Science, 305, 1933

Marshall, A.G., Verdun, F.R. 1990, Fourier Transforms in NMR, Optical, and Mass Spectrometry. A User's Handbook (Amsterdam:Elsevier)

McComas, D.J., et al. 2004, AIP Conf. Proc., 719, 162

Mitchell, D.G., Brandt, P.C., Roelof, E.C., Dandouras, J., Krimigis, S.M., Mauk, B.H. 2005, Science, 308, 989

Moore, T.E., et al. 2003, SSR, 109, 351

Witte, M., Banaszkiewicz, M., Rosenbauer, H., McMullin, D. 2004, Adv.S.R., 34, 61

Wurz, P. 2000, in The Outer Heliosphere: Beyond the Planets, ed. K. Scherer et al. (Katlenburg-Lindau: Copernicus Gesellschaft e.V.), 251

Wurz, P., Collier, M.R., Moore, T.E., Simpson, D., Fuselier, S., Lennartsson, W. 2004, AIP Conf. Proc., 719, 195

Ziegler, J.F., Biersack, J.P., Littmark, U. 1996, The stopping and range of ions in solids (New York: Pergamon Press)
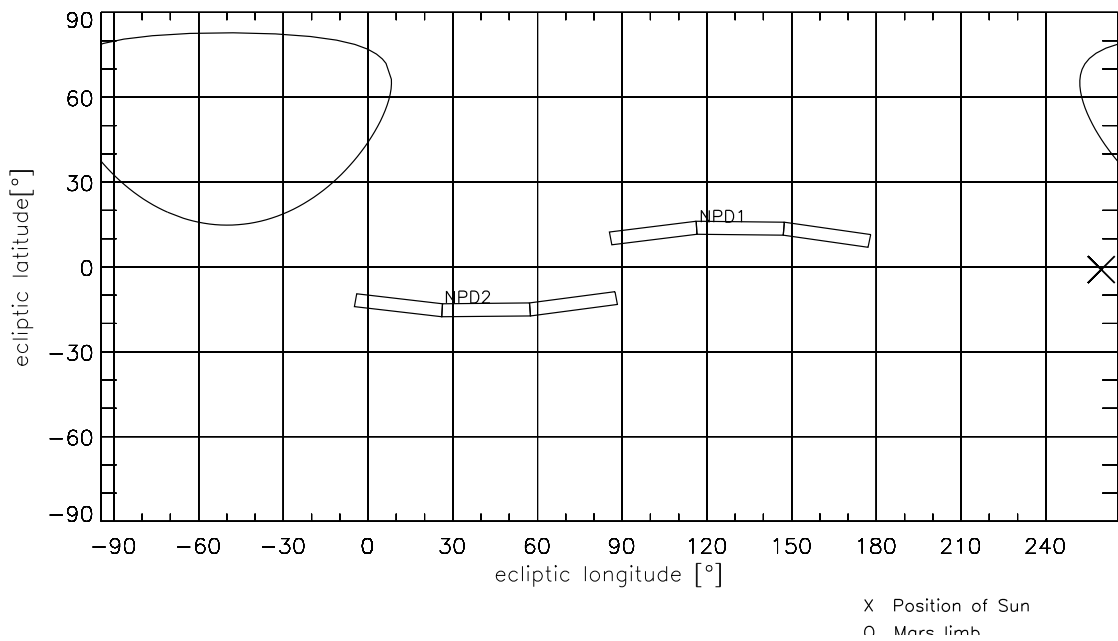
Fig. 1.— NPD observation conditions on 2004 February 24, 00:10 UT, in Mars orbit. The 2×3 elongated boxes are the fields-of-view of the two NPD sensors, each with their three angular channels (5×30° each). The position of the Sun (cross) and the Mars limb are indicated as well.
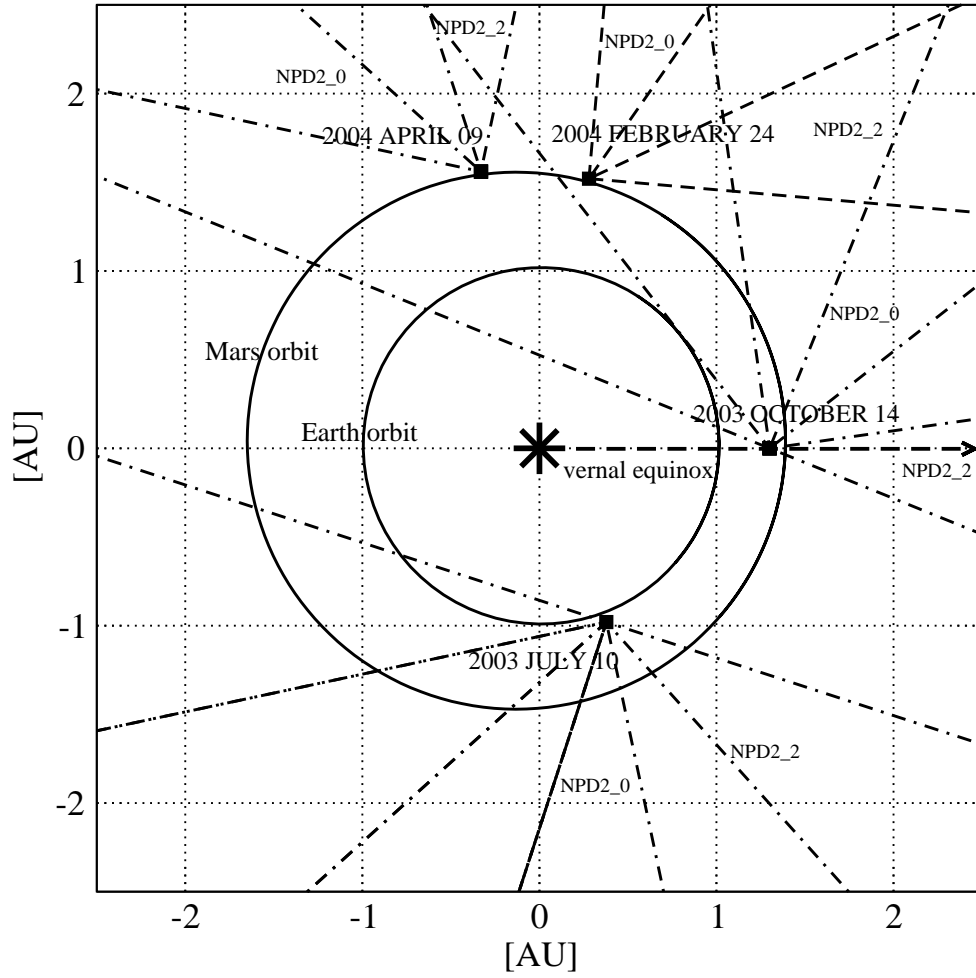
Fig. 2.— Overview of ENA observations, projected on the Earth ecliptic plane. Shown are four specific measurement locations between July 2003 and April 2004. The Mars orbit insertion took place in December 2003.
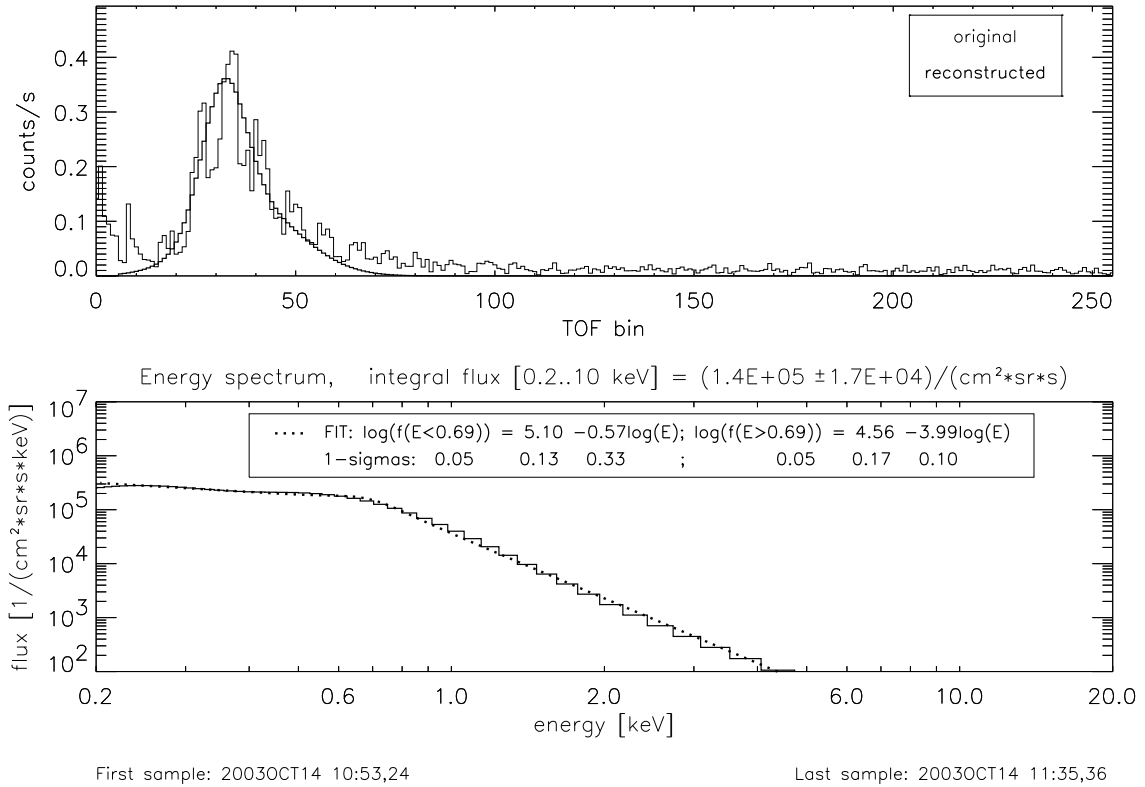
Fig. 3.— Example of a TOF spectrum for 2003 October 14, from NPD1, channel 0. Every incoming ENA is stored as a single count in one of the 256 TOF bins, each 8 nanoseconds wide. The top panel shows the original TOF spectrum (accumulated for 2000 s) and the reconstructed TOF signal after background removal and noise filtering. The bottom panel shows the energy spectrum calculated from the reconstructed TOF signal above, and a fit to this spectrum (dotted line).
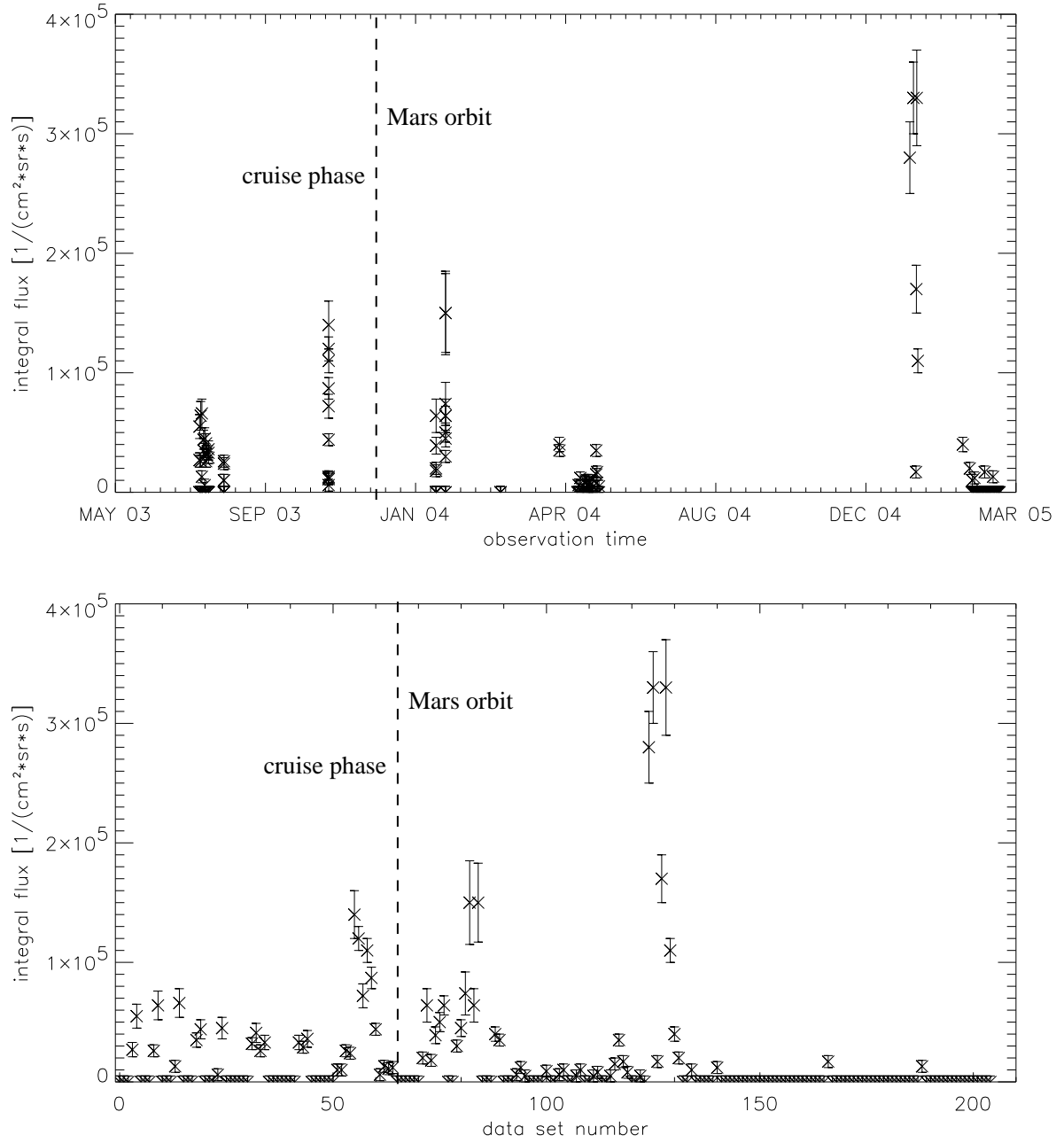
Fig. 4.— Integral flux versus observation time for all measured spectra as a function of observation time (top panel) or as a function of data set number (bottom panel). The dashed line separates the observations obtained during cruise phase from those on Mars orbit. The second half of the data set (data set number 124...204) belongs to the short time interval February- March 2005.
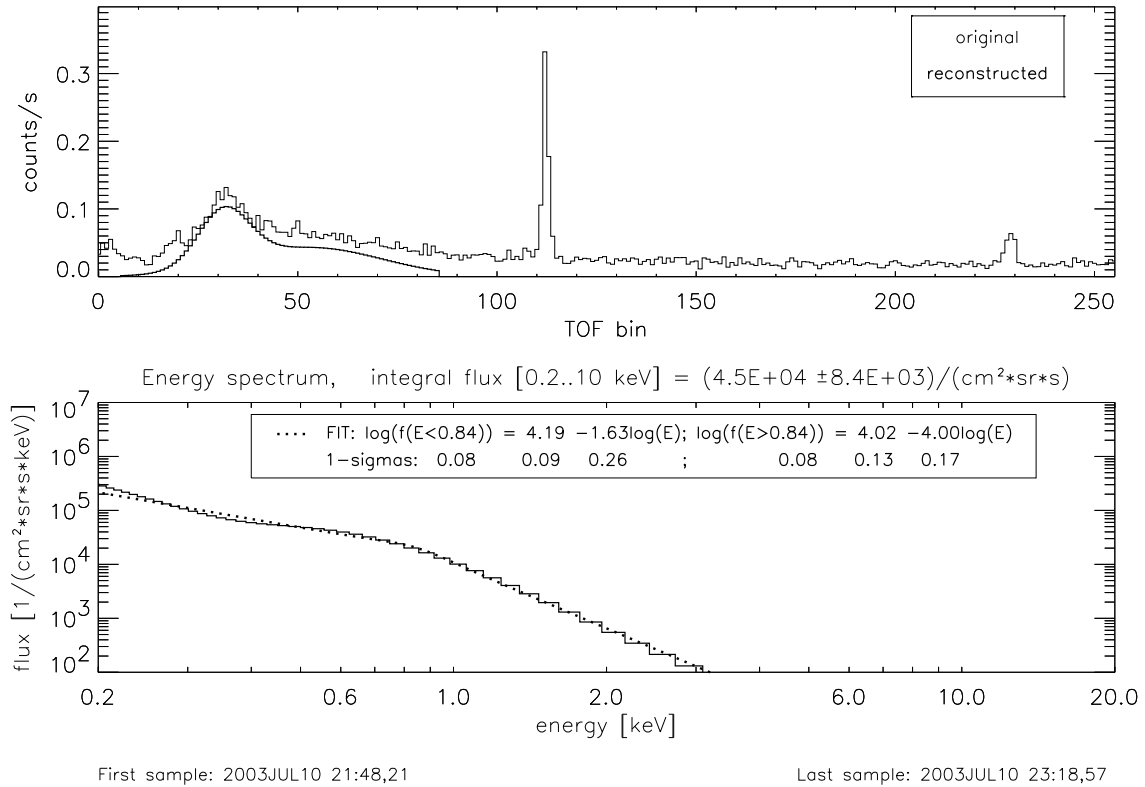
Fig. 5.— Typical example for a non-planetary ENA signal, measured during cruise phase. The data format is the same as in Figure 3. The upper panel shows the TOF spectrum, averaged over 86 minutes of data, the narrow lines at TOF bin 112 and 229 are spikes introduced by the sensor electronics. They were removed from the TOF spectrum before further analysis.
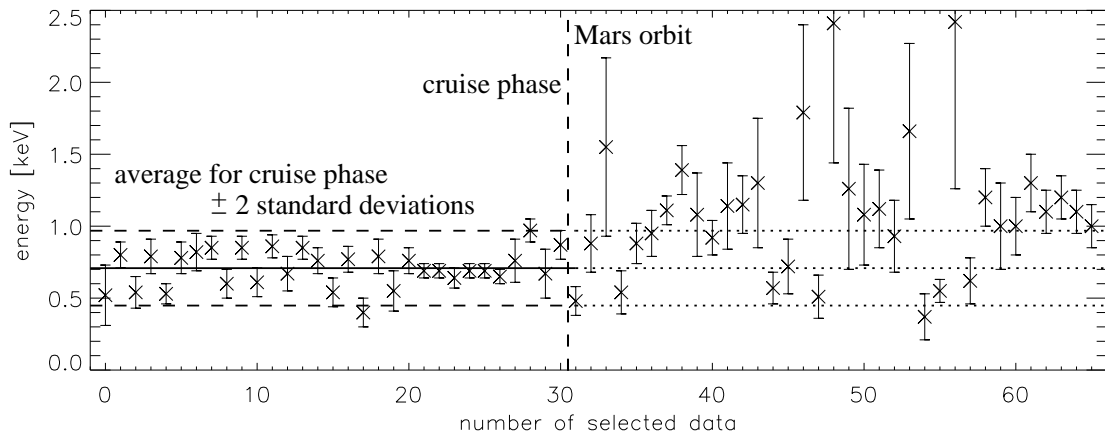
Fig. 6.— Position of roll-over of all available 66 spectra. Large error bars belong to measurements with a poor signal-to-noise ratio. The last 8 events (numbers 58 to 65) with an untypically high roll-over between 1 and 1.5 keV, all of them measured in 2005, probably have been produced by a different process.
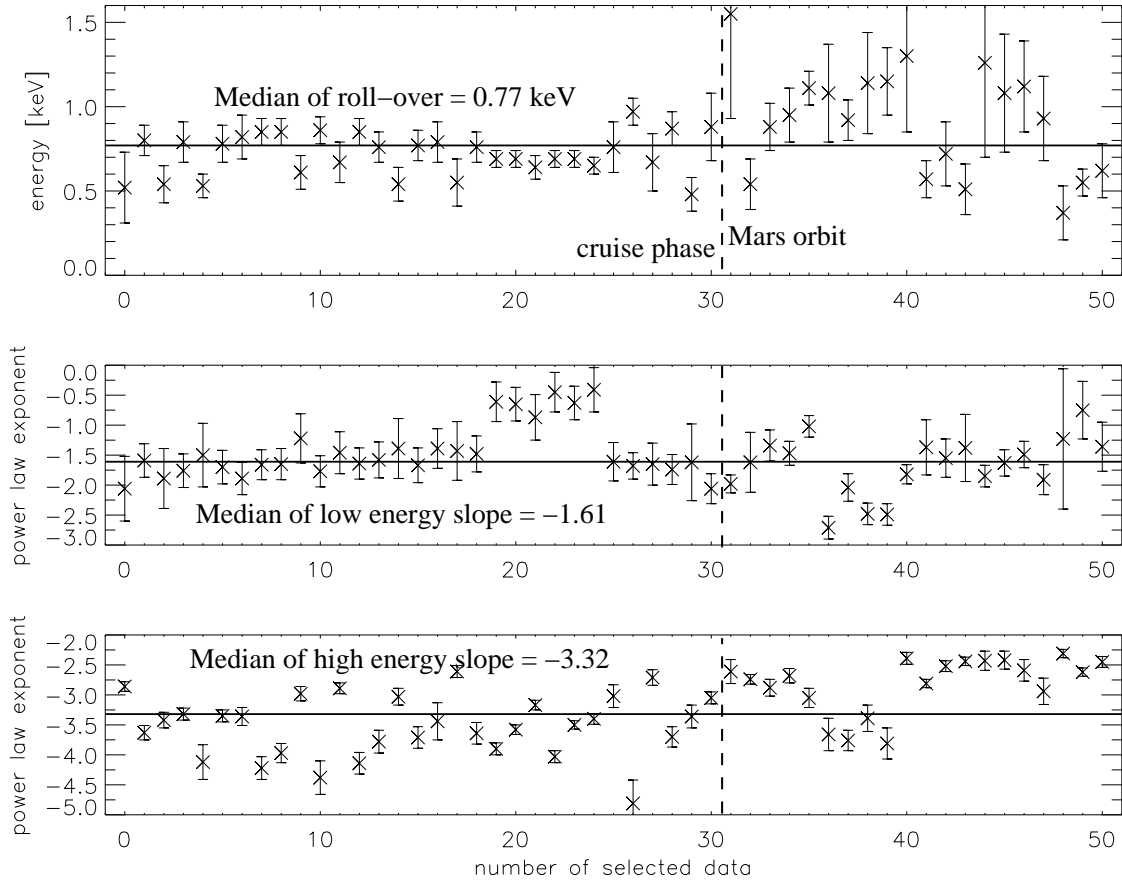
Fig. 7.— Median values of roll-over (top), low energy slope (middle), and of high energy slope (bottom) for all spectra that can be appropriately characterized by a two-composite power law.
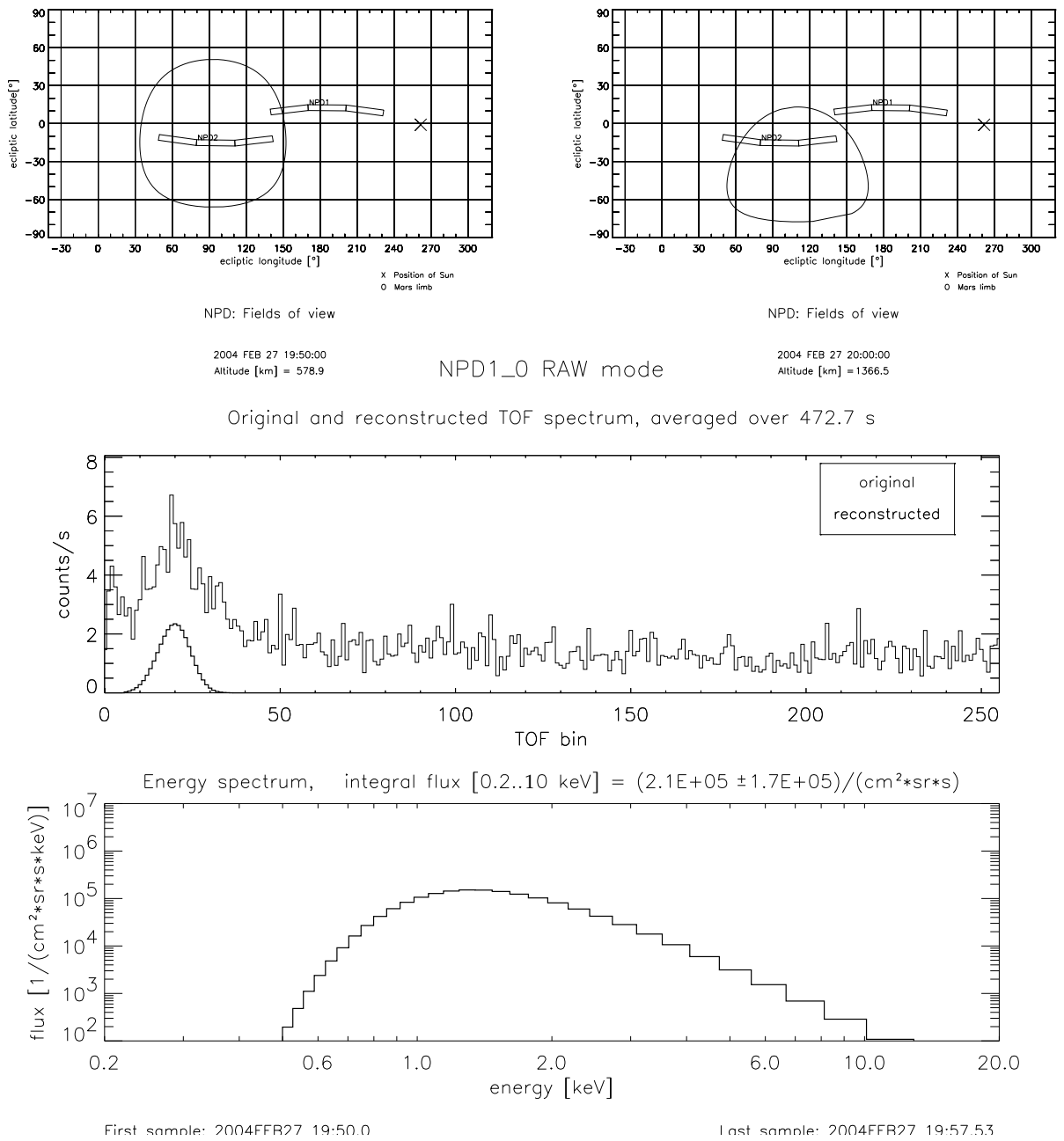
Fig. 8.— Solar wind interacting with the Martian atmosphere. The two panels at the top show the observation setting on the evening of 2004 February 27, the two lower panels show the ENAs detected from direction NPD1_0 during the observation period of 8 minutes. As the edge of the NPD1 field-of-view is near the Mars limb a distinct peak in the TOF spectrum is detected. The resulting spectrum is typical for solar wind protons that have been neutralized in the upper parts of the Martian atmosphere (see Futaana et al. (2005) for further information). It is not typical for the 51 ENA events plotted in Figure 7.
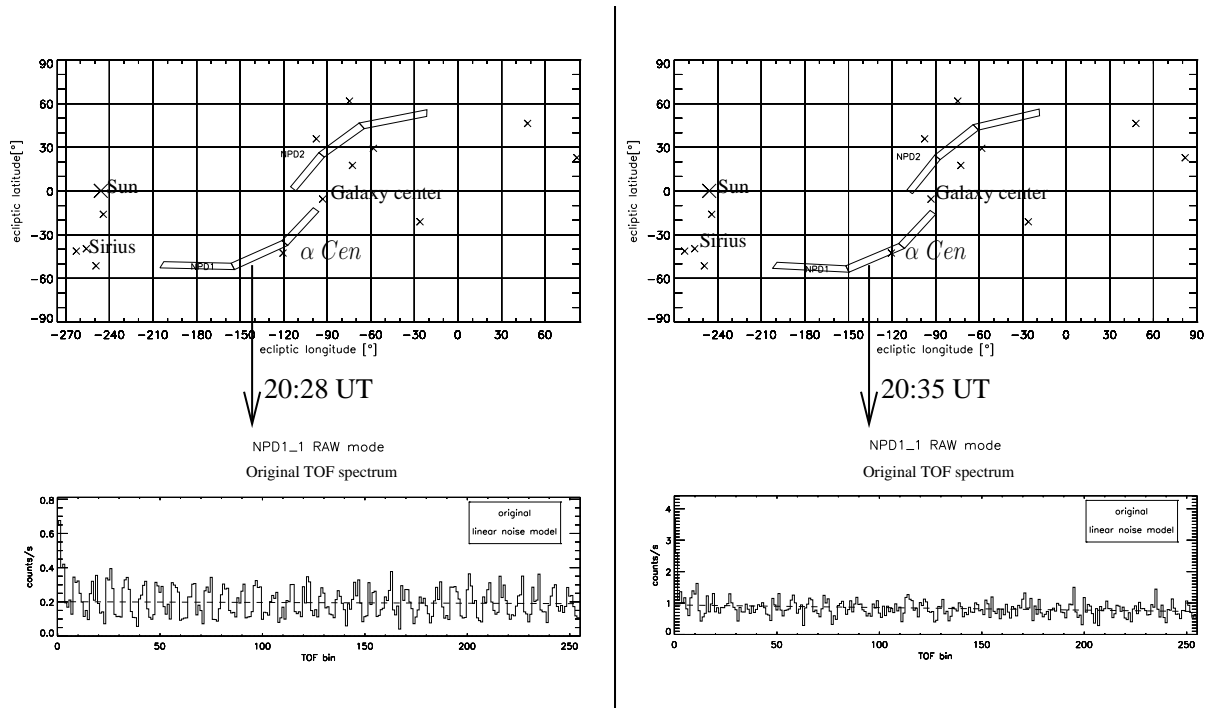
Fig. 9.— UV response of the NPD sensor. The field-of-view and the position of the brightest stars for the measurement on the evening of 2003 July 13 are shown in the top panels. On direction NPD1_1 the UV flux from α Cen raises the noise level by a factor of five in the TOF spectra (compare the bottom panels). But no TOF signal whatsoever can be seen above this background.
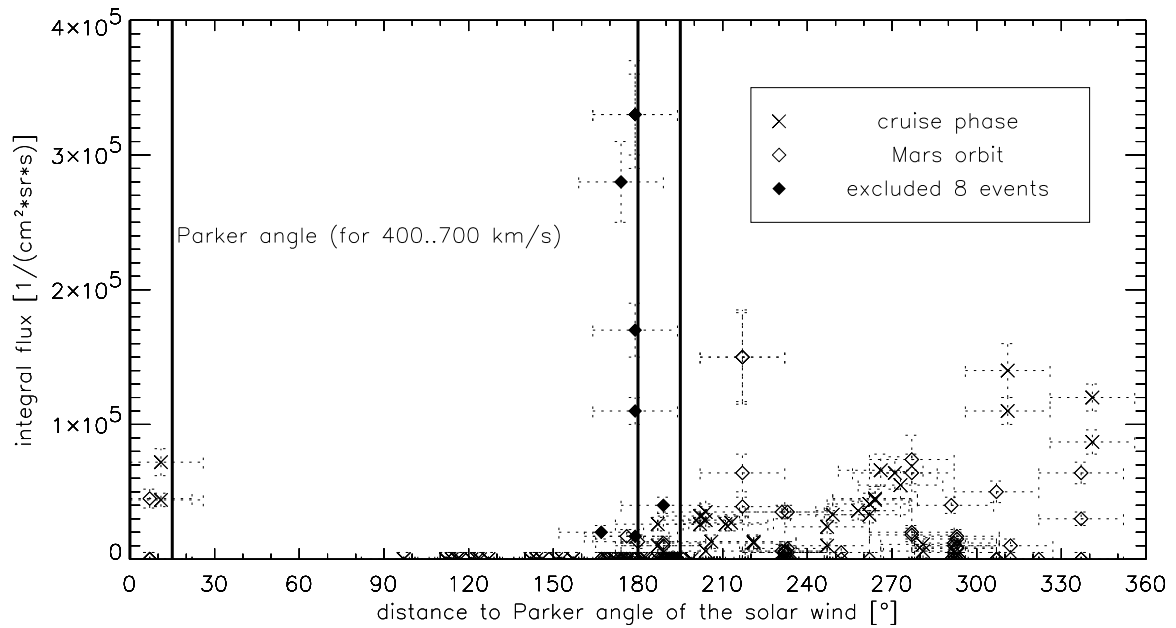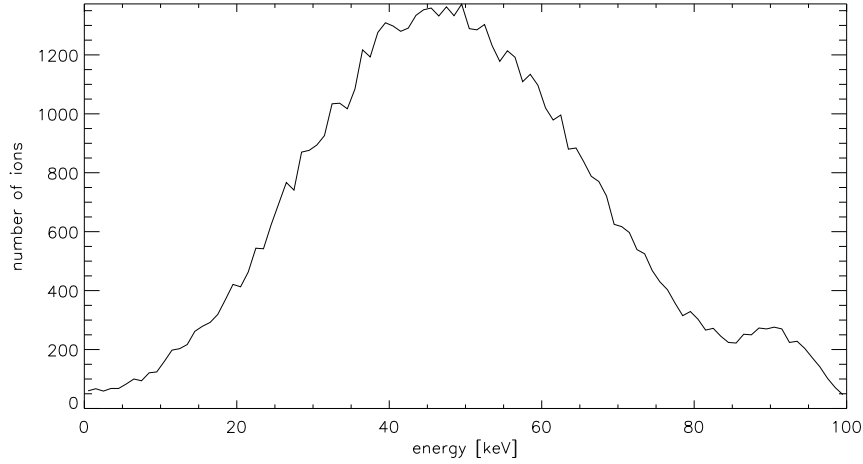
Fig. 10.— ENA flux versus pointing directions of NPD sensor for all measurements. The vertical lines indicate the range of Parker angles for varying velocities of the solar wind. The eight data points from 2005 (filled diamonds) for example lie close to the direction of particles that would follow the solar wind magnetic field, coming from the antisunward hemisphere. The interval at 0° indicates the sunward direction of the magnetic field. Data obtained during cruise phase (crosses), during Mars orbit in 2004 (diamonds), and during Mars orbit in 2005 (filled diamonds) have been distiguished, since the data from the cruise phase are the most reliable ones.
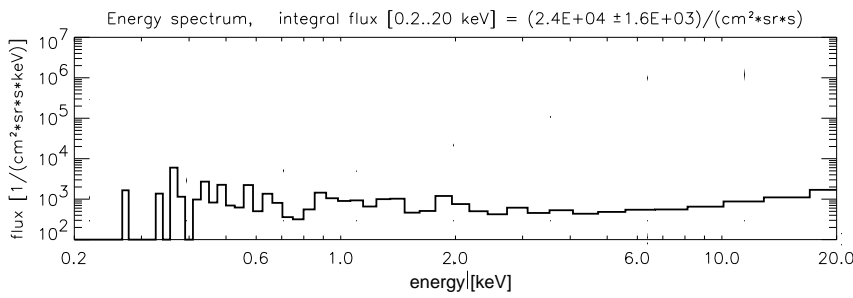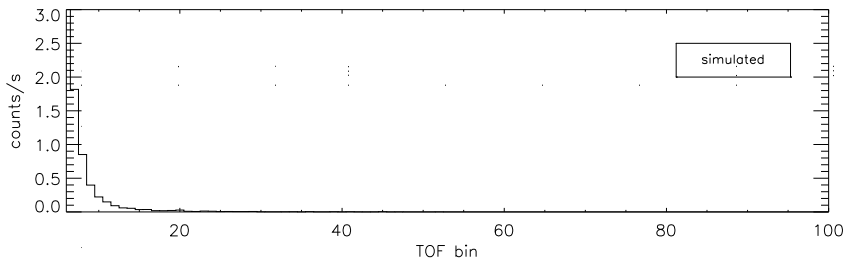
Fig. 11.— Results of a SRIM simulation with 100 keV protons backscattering on the NPD start surface. The top panel shows the energy distribution of those backscattered protons that reach the stop surface. The middle panel shows the TOF spectrum NPD would measure for such a particle source; the bottom panel shows the reconstructed energy spectrum.
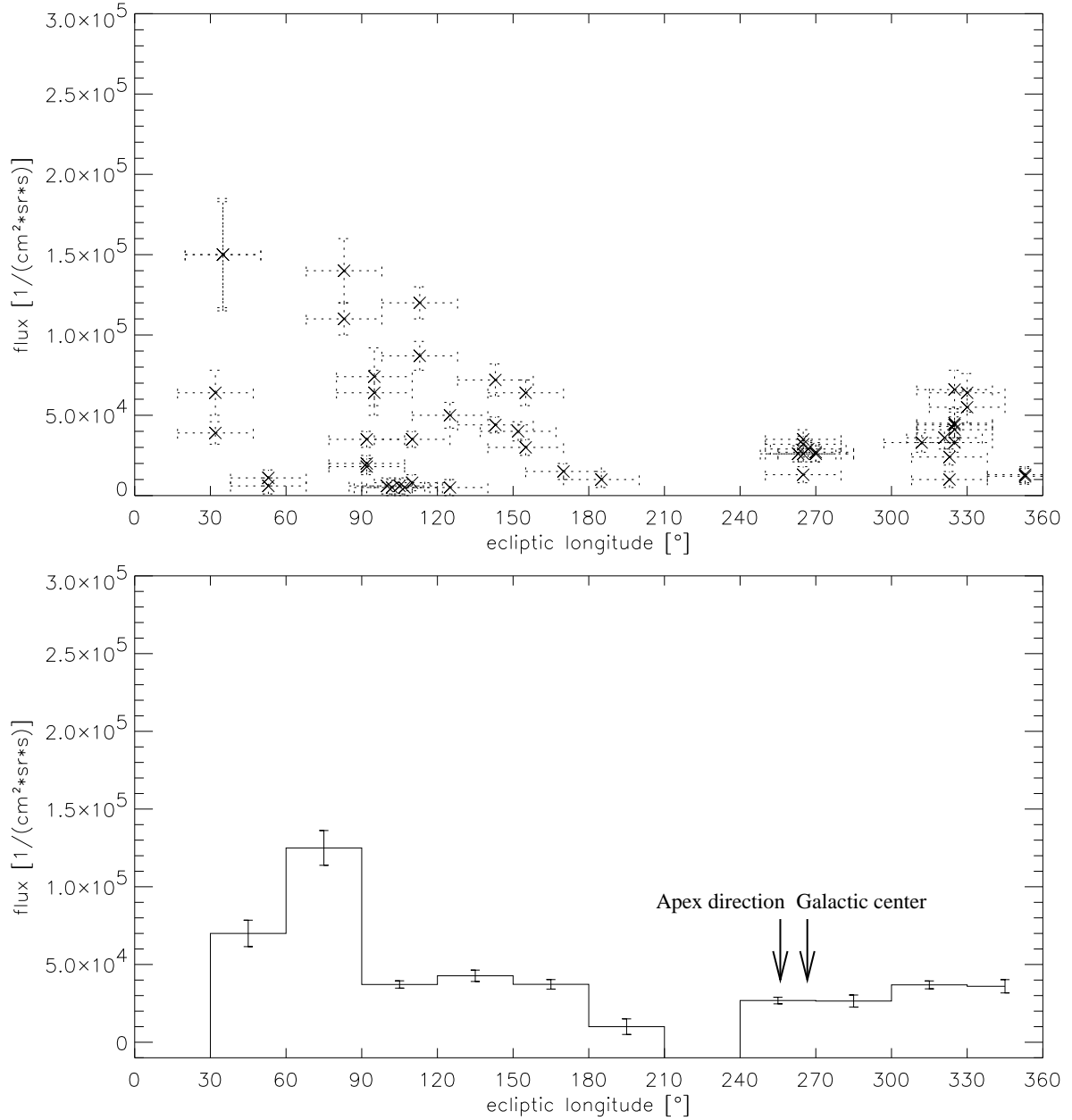
Fig. 12.— Integral ENA flux versus direction of origin. Shown are all measurements whose spectral shape fits to the class described in Section 5.3. The arrows at 255° and 267° ecliptic longitude denote the arrival direction of the interstellar neutral flow and the direction toward galactic center. The lower panel shows the data from the upper panel, redistributed into 12 bins.
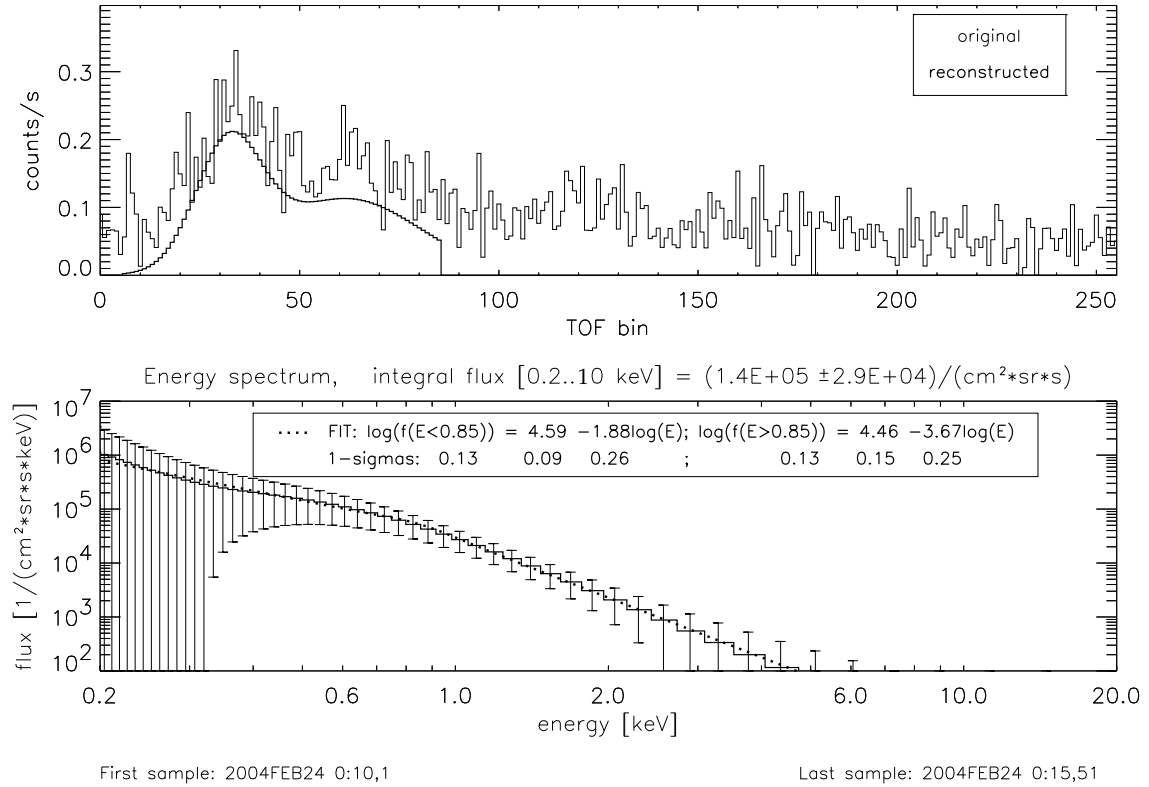
Fig. 13.— Uncertainty range of single energy bins (bottom panel) for a measured TOF signal (top panel). The data format is the same as in Figure 3, but for 2004 February 24. Note that the individual error bars may be larger than the bin values themselves.